UWB radar recognition system based on HOS and SVMs

Rahmad Sadli, Charles Tatkeu, Khadija Hamidoun, Yassin El Hillali, Atika Rivenq

IET Radar, Sonar & Navigation

Special Issue: Advanced Automotive Sensing – Towards Car Autonomy

IET Journals
The Institution of Engineering and Technology

UWB radar recognition system based on HOS and SVMs

ISSN 1751-8784
Received on 5th April 2018
Revised 23rd June 2018
Accepted on 30th July 2018
E-First on 11th September 2018
doi: 10.1049/iet-rsn.2018.5065
www.ietdl.org

Rahmad Sadli[1,2] ✉, Charles Tatkeu[2], Khadija Hamidoun[1], Yassin El Hillali[1], Atika Rivenq[1]

[1]*Université de Valenciennes, CNRS, Univé de Lille, YNCREA, Centrale Lille, UMR 8520-IEMN, DOAE, F-59313 Valenciennes, France*
[2]*University of Lille Nord de France, F-59000 Lille, IFSTTAR, COSYS, LEOST, F-59650 Villeneuve d'Ascq, France*
✉ *E-mail: rahmad.sadli@univ-valenciennes.fr*

Abstract: This study proposes an original ultra-wideband short-range radar (UWB-SRR) recognition system based on higher-order statistics (HOS) and support vector machines (SVMs). The main purpose of this work is to improve the road safety by implementing these techniques for detection and recognition of the uncovered road users such as pedestrians and cyclists. The combination of HOS and cell-averaging constant false alarm rate (CA-CFAR) radar detector has been proposed and investigated. The results show that a combination of HOS and CA-CFAR promises a good performance for UWB radar detector. The authors have also evaluated the performance of SVM-based target recognition system using normalised radar signature as input features. A total of 1000 signatures have been extracted for each class including pedestrian, cyclist, and car, where 50% of them have been used for the training data and the rest for the validation data. The results show that the SVM gives a good performance for the proposed system, where the recognition rates are up to 96.23, 95.25 and 97.23% for the cyclist, pedestrian and car. In the real testing performance using their scenarios, the system has successfully identified 92.77% of the right cyclist, 90.82% of the right pedestrian and 90.73% of the right car.

1 Introduction

One of the factors that contribute to the injuries and mortality of the uncovered road users such as pedestrians and cyclists is the lack of drivers' visibility. The blind spots around the trucks and buses environments could make a fundamental crash accident with these uncovered road users [1].

Many techniques have been proposed over the years in order to reduce these injuries and mortality caused by road crash accidents. Crash warning and avoidance systems promise a great contribution to enhance the protection of the pedestrians and the cyclists. These potential solutions include the radar system and the computer vision for object detection as suggested in [2]. However, the performance of the camera-based system will decrease when illumination diminishes, as an example in cloudy, smoggy, foggy and night conditions. On the other hand, the radar system is robust to such conditions, and it can provide accurately the distance of both stationary and moving targets while the camera cannot. By consequence, it detects and tracks their movement and can reduce this fatal error.

In this work, an original ultra-wideband short-range radar (UWB-SRR) recognition system based on higher-order statistics (HOS) and support vector machines (SVMs) has been proposed, where the normalised amplitudes are the basic elements of the features vectors.

The proposed radar system uses UWB technology in order to reach high obstacles detection. This technology is characterised by a very low-power density and a very small pulse width, from few picoseconds to few nanoseconds. The amplitude of the pulse should be normalised to comply with Federal Communications Commission mask. The wide bandwidth issued (several GHz) allows signals with a precise temporal resolution, low probability of interception/detection and offers robustness against multipath fading [3]. Thus, the UWB radar offers a great interest in short-range road safety applications [4].

The use of UWB in the SRR system presents many advantages. First, the brevity of UWB pulses with strong spectral contents makes it possible to obtain information on the target with a rich transitory response content. This allows the easy dissociation of various echoes at the reception stage. Then, the broadband spectrum authorises to obtain results on the entire frequency band in a single measurement together with a strong capacity for detection. Finally, the pulse spectrum has abilities to penetrate through naturally screening materials [5]. Considering all these properties, UWB radar using very short pulses is of great interest for many applications of obstacle detection and target identification in short range [6].

In this paper, we have explained about how the radar target is localised and identified by using, respectively, a proposed method 'a combination of HOS and the well known cell-averaging constant false alarm rate (CA-CFAR) radar detector' and SVM. The performances of the proposed radar detector and SVM target recognition based on radar signature have been analysed.

This paper is organised as follows. Section 2 introduces briefly the HOS and its variants including the fourth-order cumulant based on Tugnait4 algorithm and the fourth-order cross-moment. In Section 3, the SVM recognition technique is explained. Then, Section 4 presents in great detail about the performance of the proposed radar detector based on HOS and CA-CFAR, and it explains also how the radar signatures are collected. Section 5 presents the performance of target recognition based on SVM using the radar signatures as the input features. The last section of this paper provides the discussion and the conclusion.

2 Higher-order statistics

Unlike second-order statistics, the HOS algorithm is based on higher-order moment spectra in order to interpret and analyse the characteristics of a random process [7, 8].

This technique offers many advantages. It reduces clearly the Gaussian noise and the secondary lobes, reconstructs the phase as well as magnitude response of signals or systems and detects and characterises the non-linearity in the data. In addition, the use of HOS allows detecting several obstacles at the same time and simplifying the automation of the process by applying a simple threshold.

HOS consists of higher-order moment spectra, which is defined for deterministic signals and cumulant spectra for random process [7]. Indeed, many real-world applications are truly non-Gaussian. Therefore, contrary to the second-order statistics, HOS is

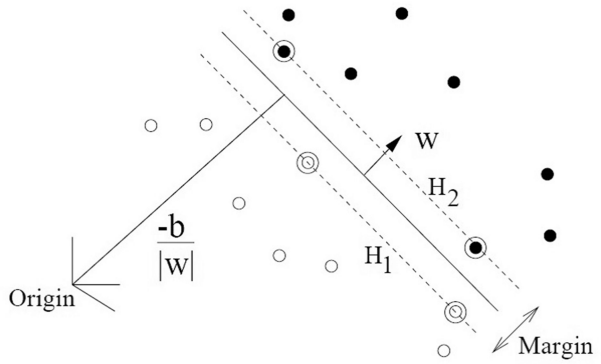

Fig. 1 *Illustration of support vectors, hyperplane and margin*

applicable when we are dealing with non-Gaussian, because it can adapt to non-Gaussian noise or to non-linear channel characteristics and reveal the phase information [8, 9]. In [10], they used the HOS method to estimate time delay in unknown spatially correlated noise and the result is better than that of used cross-correlation method.

There are two algorithms of the HOS that have been investigated in this work: the fourth-order cumulant based on Tugnait4 algorithm and the fourth-order cross-moment.

2.1 Tugnait4 algorithm

Tugnait4 is an algorithm which uses the fourth-order cumulant of the HOS to estimate time delay. It is developed by Tugnait (1989). The advantage of the Tugnait4 algorithm is its ability to suppress the Gaussian noise over the useful signal. The expression of the Tugnait4 algorithm is shown in the equation below [4, 10]:

$$\boldsymbol{J}_4(i_0) = \frac{\mathbf{cum}_4(c(i-i_0),\, c(i-i_0),\, r(i),\, r(i))}{\sqrt{|\mathbf{cum}_4(c(i),\, c(i))|\,|\mathbf{cum}_4(r(i),\, r(i))|}} \tag{1}$$

with c as the reference signal, r as the incoming signal and i_0 as the time index decision where (see (2)) .

2.2 Fourth-order cross-moment

A novel design based on the approach of a fourth-order cross-moment is proposed in this UWB radar. The fourth-order cross-moment m_4 for a stationary random process $x(n)$ with samples $x_0(n)$, $x_1(n)$, $x_2(n)$ and $x_3(n)$ is defined as [7]

$$m_4(\tau_1,\, \tau_2,\, \tau_3) = E\{x_0(n)x_1(n+\tau_1)x_2(n+\tau_2)x_3(n+\tau_3)\} \tag{3}$$

where $E\{*\}$ denotes statistical expectation.

For deterministic signal, it is replaced by a time summation over all time samples (for energy signals) or time averaging (for power signals). Under the assumption that $x(n)$ is of zero mean, the fourth-order cross-moment is calculated from the given data as [7]

$$m_4(\tau_1,\, \tau_2,\, \tau_3) = \frac{1}{N}\sum_{n=0}^{N} x_0(n)x_1(n+\tau_1)x_2(n+\tau_2)x_3(n+\tau_3) \tag{4}$$

where N is the length of the signal.

A better combination of the x_0, x_1, x_2 and x_3 for the proposed system is 'Reference', 'Signal', 'Reference' and 'Signal', respectively. Then, 'x_0, x_2' are replaced by the received echoes and 'x_1, x_3' are replaced by the references. The parameters of τ_1 is equal to zero, and $\tau_2 = \tau_3 = \tau$ so the equation becomes

$$m_4(\tau_1,\, \tau_2,\, \tau_3) = \frac{1}{N}\sum_{n=0}^{N} [c(n)r(n+\tau)]^2 \tag{5}$$

with c as the reference signal and r is the received signal.

After looking briefly at the HOS, then in the next section, we explain the literature of basic SVM concept.

3 Support vector machine

SVM is a supervised machine learning of binary classification technique for pattern recognition. This classifier creates a hyperplane to separate the pattern of data into two classes (+1 or −1) with the maximum margin. The vectors that define the hyperplane are called *support vectors* [11] (Fig. 1).

Let us label the training data $\boldsymbol{x}_i \in R^{\mathrm{d}}$ with a label $\boldsymbol{y}_i \in -1, 1$, for all the training data $i = 1, \ldots, n$, where n is the number of data and d is the dimension of the problem. $\boldsymbol{y}_i$ is separated by a hyperplane with margin M, then for each training sample $(\boldsymbol{x}_i, \boldsymbol{y}_i)$

$$\text{negative class } \boldsymbol{w}^{\mathrm{T}}\boldsymbol{x}_i + b \le -1, \text{ if } \boldsymbol{y}_i = -1$$

$$\text{positive class } \boldsymbol{w}^{\mathrm{T}}\boldsymbol{x}_i + b \ge 1, \text{ if } \boldsymbol{y}_i = 1$$

To maximise the margin, we need to minimise $\| \boldsymbol{w} \|$. That is equivalent to minimise $1/2 \| \boldsymbol{w} \|^2$. Then, we can formulate a quadratic optimisation problem and solve it for $\boldsymbol{w}$ and b.

By multiplying each class by its label, then we have the constrain of this Quadratic Programming (QP) optimisation as

$$\boldsymbol{y}_i(\boldsymbol{w}^{\mathrm{T}}\boldsymbol{x}_i + b) \ge 1 \tag{6}$$

Thus, the optimal margin can then be found by minimising

$$1/2 \| \boldsymbol{w} \|^2 \tag{7}$$

which subjects to

$$\boldsymbol{y}_i(\boldsymbol{w}^{\mathrm{T}}\boldsymbol{x}_i + b) - 1 \ge 0, \quad \forall i \tag{8}$$

3.1 Solving optimisation problem

By using the Lagrange multiplier method, we get the primal form for this minimisation problem

$$L = f(x) - \alpha\, g(x) \tag{9}$$

where $g(x) \ge 0$.

Inserting $f(x) = 1/2 \| \boldsymbol{w} \|^2$ and $g(x) = \boldsymbol{y}(\boldsymbol{w}^{\mathrm{T}}\boldsymbol{x}_i + b) - 1$ into (9), we get the primal form

$$L_{\mathrm{p}} = 1/2 \| \boldsymbol{w} \|^2 - \sum_{i=1}^{n} \alpha_i(\boldsymbol{y}_i(\boldsymbol{w}^{\mathrm{T}}\boldsymbol{x}_i + b) - 1) \tag{10}$$

By applying the Karush–Kuhn–Tucker conditions to the primal form, we get the primal-dual form

$$\begin{aligned}\mathbf{cum}_4(c(i-i_0),\, c(i-i_0),\, r(i),\, r(i)) = {} & \frac{1}{N}\sum_{i=1}^{N-1} c^2(i-i_0)r^2(i) \\ & -2\left[\frac{1}{N}\sum_{i=0}^{N-1} c(i-i_0)r(i)\right]^2 \\ & -\left[\frac{1}{N}\sum_{i=0}^{N-1} c^2(i-i_0)\right]\left[\frac{1}{N}\sum_{i=0}^{N-1} r^2(i)\right]\end{aligned} \tag{2}$$

$$L_{\text{pd}} = -1/2\sum_{i=1}^{n}\sum_{j=1}^{n}\alpha_i\alpha_j y_i y_j \boldsymbol{x}_i\boldsymbol{x}_j + \sum_{i=1}^{n}\alpha_i \tag{11}$$

As the vectors $\boldsymbol{x}_i$, $\boldsymbol{x}_j$ and $\boldsymbol{y}_i$ are known and L_{pd} is optimal at $(\partial L_{\text{pd}}/\partial\alpha) = 0$, and at $\sum_{i=1}^{n}\alpha_i y_i = 0$, we can find α_i value.

The non-negative value of α_i will correspond to support vectors. Knowing the α_i, we can find $\boldsymbol{w}$ by

$$\boldsymbol{w} = \sum_{i=1}^{n}\alpha_i \boldsymbol{y}_i \boldsymbol{x}_i \tag{12}$$

The b parameter can then be determined by the next equation

$$\alpha_i[\boldsymbol{y}_i(\boldsymbol{w}^{\text{T}}\boldsymbol{x}_i + b) - 1] = 0 \tag{13}$$

3.2 SVM kernel

In the case of non-linear separable data, the transformations are performed by using variable kernel functions such as sigmoid, polynomial, linear, Gaussian radial basis function (RBF) etc. These kernel functions define an inner product in high-dimensional space, given as below [12]:

$$\text{linear}\, K(\boldsymbol{x}_i, \boldsymbol{x}_j) = \boldsymbol{x}_i^{\text{T}}\boldsymbol{x}_j \tag{14}$$

$$\text{polynomial}\, K(\boldsymbol{x}_i, \boldsymbol{x}_j) = (\gamma \boldsymbol{x}_i^{\text{T}}\boldsymbol{x}_j + r)^{\text{d}},\ \gamma > 0 \tag{15}$$

$$\text{RBF}\, K(\boldsymbol{x}_i, \boldsymbol{x}_j) = \exp(-\gamma \parallel \boldsymbol{x}_i - \boldsymbol{x}_j \parallel^2),\ \gamma > 0 \tag{16}$$

$$\text{sigmoid}\, K(\boldsymbol{x}_i, x_j) = \tanh(\gamma \boldsymbol{x}_i^{\text{T}}\boldsymbol{x}_j + r) \tag{17}$$

The SVM technique was realised by using the library for SVM (LIBSVM) developed by [13]. LIBSVM is a library for SVM that has been widely used in many research areas. These four basic kernels are investigated and their performances are compared in order to have a better kernel that matches in our UWB-SRR system.

4 Target detection based on HOS

4.1 Hardware specifications

The experimentation has been performed by using an UWB Radar Kit HST-D3 hardware module developed by UMAIN.INC, which is a short range of UWB impulse radar that packs 450 MHz–1 GHz of radio-frequency bandwidth in a small, low-cost, low-power device. This UWB commercial radar module, embedded with in-house developed software is connected to a Raspberry-Pi3 which stored the raw radar data.

UWB HST-D3 radar module comes with two types of antennas, *UWB directional antenna* and *UWB monopole antenna*, but in our experiments, we use the *UWB directional antenna* because it has better target echo-to-clutter and noise ratio. Detail specification of the radar module is presented in Table 1.

4.2 Experimental setup

All of the experiments were conducted yet in the parking area of our laboratory. The radar was attached on a tripod and placed on a stroller. The height of the radar from the ground is about 1.8 m. Fig. 2 illustrates more detail about this radar setup. The distance of the targets is within the range of 0.5–8 m far from the radar. For this first experimentation, the scenario for identification of the pedestrian and the cyclist is: both pedestrian and cyclist can move randomly in front of the stationary radar within the range mentioned above (from 0.5 to 8 m far from the radar). The pedestrian speed varies from 3 to 5 km/h, and the cyclist speed is 6–10 km/h.

The experimentation scenario for the car identification is as follows: we performed the experiments on the stationary of three different cars while the stroller with the radar is moving toward and backward to the cars with the speed was from 4 to 5 km/h. For this preliminary experimentation, the velocity of the cars is not our main purpose, but we focus on the nature of the target.

Table 1 Specification of radar sensor module HST-D3 [14]

Parameter	Value	Comments
detection range	10–20 m	factory default 13.4 m
frequency range	3–4 GHz	
bandwidth	0.45–1 GHz	max: 1 GHz
output rower	typ. −25 dBm	
distance resolution	15–33 cm	

Fig. 2 *Radar setup and an example of an experiment where a cyclist moved in front of the radar*

4.3 Time-delay estimation

Determination of radar targets requires the time-delay estimation in order to localise the targets positions. Therefore, in this section, we first present the investigation results of the performance comparison between two HOS methods including the fourth-order cumulant (Tugnait4-based algorithm) and the fourth-order cross-moment. Then, we provided the results of a comparison between the selected HOS and the ordinary second-order statistics.

Fig. 3 shows an example of the performance of the fourth-order cumulant (green curve) and the fourth-order cross-moment (red-dotted curve). Both methods were applied to the original echo of raw radar data. It can be seen that they have a very similar performance in terms of noise suppression. Therefore, since the fourth-order cross-moment has less computation than that of the fourth-order cumulant, it is better to use the fourth-order cross-moment in estimating time delay in UWB radar system. Then, the fourth-order cross-moment is compared with the ordinary second-order statistics as presented in Fig. 4. From this figure, we can see that the first target has a lot of reflections of energy which is easy to be detected, whereas the second one only has very few reflections of energy which is difficult to be detected. Red curve and blue-dotted curve in this figure are the plots of HOS result and the plot of the ordinary second-order result, respectively. We can see that with the threshold value set to 0.05 (black-dotted line), HOS positively detected the position of the second target, thanks to its successful noise suppression, while the second-order statistics

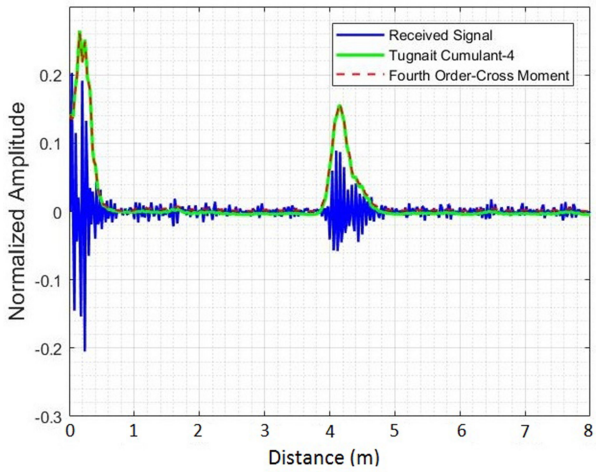

Fig. 3 *Performance comparison between the fourth-order cumulant (Tugnait4) and the fourth-order cross-moment*

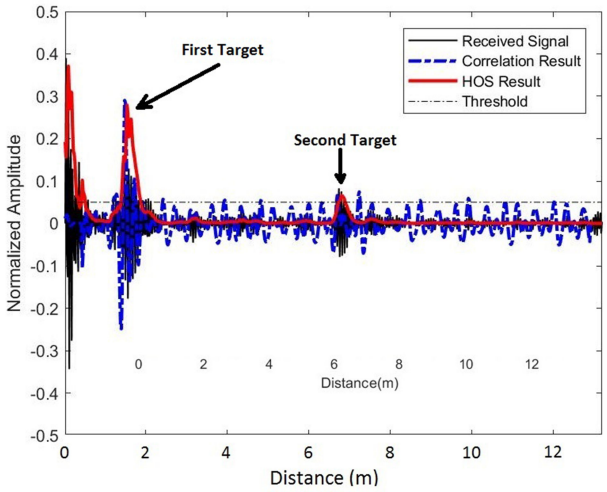

Fig. 4 *Comparison result between HOS and ordinary second-order statistics in the presence of two radar targets with the threshold value set to 0.05*

Table 2 Transfer function for several higher orders of pulse canceller [15]

Number of pulses processed	Transfer function
2	$1 - z^{-1}$
3	$1 - 2z^{-1} + z^{-2}$
4	$1 - 3z^{-1} + 3z^{-2} - z^{-3}$
5	$1 - 4z^{-1} + 6z^{-2} - 4z^{-3} + z^{-4}$

produced a lot of false detection and it failed to detect the second target.

From this observation, we concluded that one of the advantages of using HOS in this radar application is that it can enhance the radar sensitivity performance, thanks to its ability to suppress the noise.

In the next section, we investigated the comparison performance between HOS and the well known detector CFAR. We proposed to combine HOS and CFAR in order to have a robust radar target detector. We continued this discussion by introducing a moving target indication (MTI).

4.4 Moving TI

An MTI helps for pre-processing the radar signal before applying targets detection method because it can enhance the signal-to-clutter ratio of the radar echo. One of the MTI methods is the so-called pulse canceller. The basic pulse canceller is 2-pulse

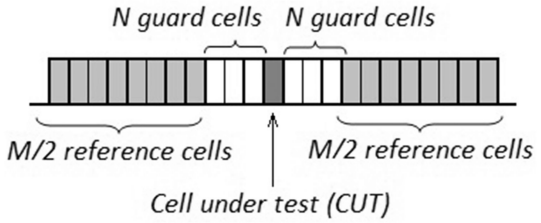

Fig. 5 *CA-CFAR algorithm architecture [17]*

canceller. To have a higher order of this pulse canceller, we can cascade the 2-pulse canceller [15]. Transfer functions for several higher-order pulse cancellers are presented in Table 2.

On the basis of [16] it is shown that the 4-pulse canceller performs effective reduction of static radar clutters, so in this experiment before implementing HOS and CFAR detector, we simply applied the 4-pulse canceller to reject the clutters and direct antenna coupling in our UWB radar. The 4-pulse canceller can be written as

$$R_{\text{out}} = R_i - 3R_{i-1} + 3R_{i-2} - R_{i-3} \tag{18}$$

where R_{out} is the final output after pulse canceller, R_{i} is the input original signal and $R_{\text{i}-n}$ is the nth original delayed signal.

4.5 HOS and CFAR combination

We began this section by introducing the well known CFAR detector and then continued by presenting the performance comparison results between the selected HOS type (the fourth-*order cross-moment*) and the CFAR detector. The most known good performance of CFAR is the CA-CFAR.

In a CA-CFAR detector, a threshold is adaptively estimated based on local information on the background noise, from both leading and lagging cells (called reference cells) surrounding the cell under test [17–19].

The noise estimate can be computed as [18, 19] (Fig. 5)

$$P_n = \frac{1}{M}\sum_{m=1}^{M} x_m \tag{19}$$

where M is the number of reference cells and x_m is the sample in each reference cell and P_n represents the estimated noise power. Then, the detection threshold T is given by

$$T = \alpha P_n \tag{20}$$

α is a scaling factor called the threshold factor and is calculated as

$$\alpha = M(P_{\text{fa}}^{-1/M} - 1) \tag{21}$$

where P_{fa} is the desired false alarm rate.

As already mentioned above, we have investigated the performances comparison results between automatic threshold CA-CFAR which is directly implemented in the radar signal without time-delay estimation and the HOS with the fixed threshold value. Here, we noted that both HOS and CA-CFAR are implemented after pulse canceller. We obtain that the HOS with the fixed threshold value gives better performance than that of the CA-CFAR which is directly implemented in the signal without time-delay estimation as we can see in Table 3.

We noted that the problem with CA-CFAR is the difficulty to determine the number of reference cells as shown in Figs. 6 and 7. Fig. 6 shows the result of applying CA-CFAR directly on the radar signal without time-delay estimation when the number of reference cells (M), the number of guard cells (N) and the false alarm rate (P_{fa}) were, respectively, set to, 80, 2 and 10^{-5}. With this configuration, the detector detected three targets, while in the real condition it was presented only one target at 5 m away from the radar. This means that the false alarms have occurred. Fig. 8 shows

Table 3 Performance evaluation between HOS with the fixed threshold (TH), CA-CFAR without time-delay estimation and CA-CFAR after time-delay estimation by HOS ($N = 2$, $P_{fa} = 10^{-5}$)

Detector type	Number of true detection	Number of false detection	Detection accuracy, %
HOS (TH = 0.05)	124	76	62.0
HOS (TH = 0.1)	**129**	71	**64.5**
CA-CFAR ($M = 100$)	102	98	51.0
CA-CFAR ($M = 150$)	115	85	57.5
CA-CFAR ($M = 200$)	**118**	**82**	**59.0**
CA-CFAR ($M = 250$)	106	94	53.0
HOS–CA-CFAR ($M = 100$)	157	43	78.5
HOS–CA-CFAR ($M = 150$)	164	36	82.0
HOS–CA-CFAR ($M = 200$)	**175**	**25**	**87.5**
HOS–CA-CFAR ($M = 250$)	172	28	86.0

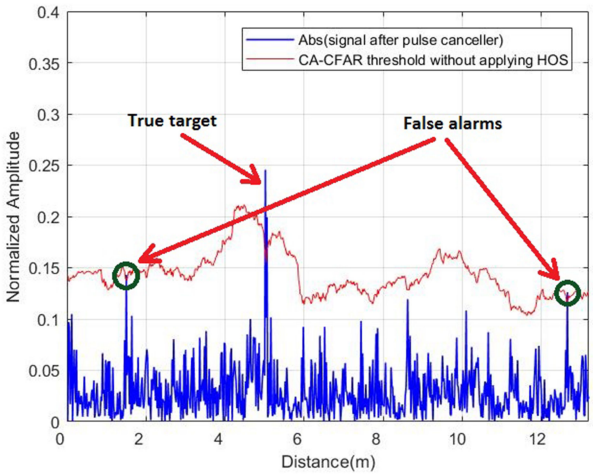

Fig. 6 *CA-CFAR detects false alarms, $P_{fa} = 10^{-5}$, $M = 80$ and $N = 2$*

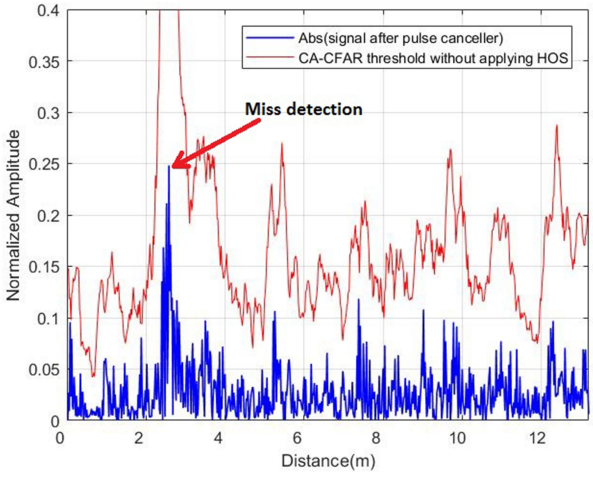

Fig. 7 *Miss detection of CA-CFAR, $P_{fa} = 10^{-5}$, $M = 20$ and $N = 2$*

the result of the CA-CFAR performance with the same number of guard cells and the false alarm rate as in the previous configuration, but the number of reference cells was reduced to 20. With this configuration, the detector performed well. It can detect the right target position without false detection, but it had the problem for another radar data frame as shown in Fig. 7 that the detector has missed detection of the presented target. Therefore, if

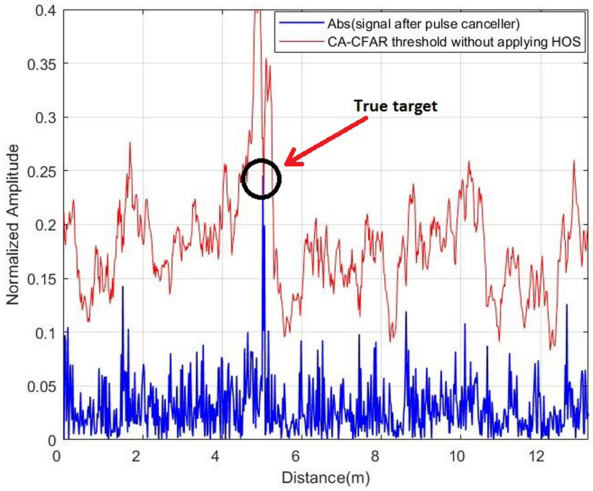

Fig. 8 *Correct detection of CA-CFAR, $P_{fa} = 10^{-5}$, $M = 20$ and $N = 2$*

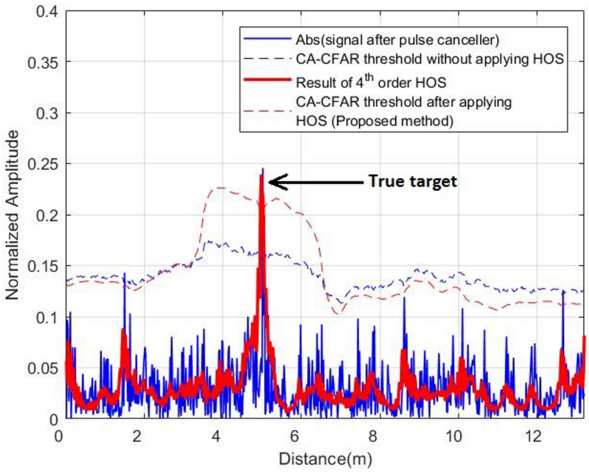

Fig. 9 *Comparison of the CA-CFAR performance run directly on the signal without time-delay estimation and with time-delay estimation (HOS), $P_{fa} = 10^{-5}$, $M = 150$ and $N = 2$. A real target presents 5 m away from the radar*

the number of reference cells is not well chosen, the detector will result in a lot of false alarms and most probably will have missed detection of the target.

To have a robust radar detector, the authors proposed a solution for this problem, that is, by first implementing the HOS to estimate the time delay before running automatic threshold CA-CFAR detector. Figs. 9–11 show several examples of the comparison results between the CA-CFAR run directly on the signal without time-delay estimation and with time-delay estimation (HOS). We can see clearly that the implementation of the CA-CFAR detector after time-delay estimation by HOS promises a better performance compared with the CA-CFAR detector without estimating the time delay.

To validate the proposed method, we have tested a number of 200 raw radar data where each of it contains a real single target. We consider two conditions including positive condition (PC) and negative condition (NC). The PC is when the radar gives the good decision, and otherwise is for the NC. The following is the detail description for both decisions:

PC:

(a) *when real condition presents one target and the observation only detects one target; that means there is no false detection and*
(b) when real condition presents no target and the observation results no detected target.

NC:

(a) *when real condition presents one target, but the observation results in more than one target, that means there are detection errors (false alarm);*
(b) *when real condition presents one target, but the observation results in no detected target; and*
(c) *when real condition presents no target, but the observation results in one or more targets.*

The performance of accuracy is calculated as

$$\text{ACC} = \frac{\text{number of PC}}{\text{number of PC} + \text{number of NC}} \times 100\% \qquad (22)$$

Table 3 presents the performance evaluation results between HOS with the fixed threshold value (TH), CA-CFAR without time-delay estimation and CA-CFAR after time-delay estimation by HOS for different numbers of the reference cells M. The number of guard cells N and the false alarm rate P_{fa} are, respectively, set to 2×10^{-5}. From this table, we can note that the performance of the HOS with the fixed threshold value is better than that of the CA-CFAR which is directly implemented in the signal without time-delay estimation, but the performance of CA-CFAR after estimating time delay by HOS outperforms the others. The detection accuracy of HOS with the fixed threshold value is up to 64.5%, when threshold value (TH) is set to 0.1, where the CA-CFAR is only up to 59.0% when the reference cell (M) is set to 200. It is clear that, the combination of HOS and CA-CFAR promises the good performance that has achieved up to 87.5% of the detection accuracy when M is set to 200..

4.6 Target detection and radar signature

After investigating the performance of the radar detectors, we noted that the combination of HOS and CA-CFAR (a proposed method) promises a good performance in UWB target detection. Then, we use this proposed method in our UWB-SRR system to detect the positions of the radar targets. The HOS is first applied after pulse canceller, and then the threshold value is estimated by using CA-CFAR on the result of the HOS. Once the position of the target is obtained, then we step back to the originally received echo and perform the windowing around the known target position and keep it as a radar signature. This signature can be directly used in real-time radar identification or can be saved to be used as the radar dataset (Fig. 12).

Fig. 13 shows three different UWB pulses distortion by three different targets of nature including pedestrian, cyclist and car. These differences in pulses' distortion are called radar target signatures. Fig. 14 shows their normalised radar signatures followed by their power spectral densities. We can see clearly the difference between them. The important things of these signatures are their normalised amplitudes that represent the features vector of each signature.

5 SVM-based radar target identification

The recognition system has been developed by using SVM technique. SVM recognises the target based on the result of the training parameters.

5.1 Dataset

In the case of UWB radar, we cannot find the dataset benchmark of radar signatures, thus we performed our own dataset. For pedestrian and cyclist, the target signatures are collected from the moving, either pedestrian or cyclist randomly with a different orientation (e.g. front, back, side etc.) in front of radar with different speed motions as already mentioned in Section 4.2. For collecting car signatures, we simply moved the radar closer to and farther away from the cars. Then, to extract the signature, we applied the method explained in Section 4.6. To have a reliable dataset, we have also considered for short stop target. We have performed the experiments to extract 1000 radar signatures for each category of a radar target.

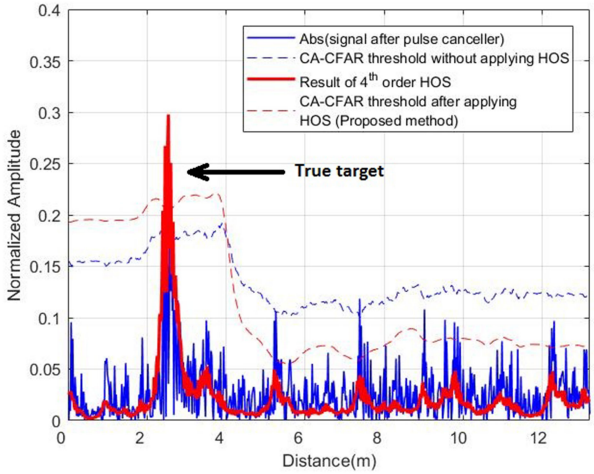

Fig. 10 *Comparison of the CA-CFAR performance run directly on the signal without time-delay estimation and with time-delay estimation (HOS), $P_{fa} = 10^{-5}$, $M = 150$, and $N = 2$. A real target presents 2.5 m away from the radar*

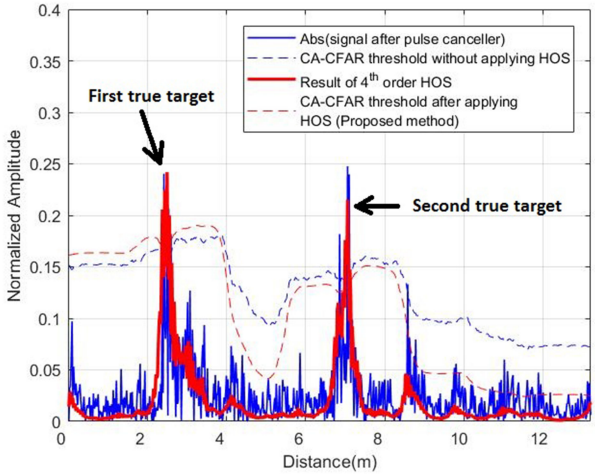

Fig. 11 *Comparison of the CA-CFAR performance run directly on the signal without time-delay estimation and with time-delay estimation (HOS), $P_{fa} = 10^{-5}$, $M = 150$ and $N = 2$. Two real targets present at 2.5 and 7 m away from the radar*

Fig. 12 *Diagram of determination of target radar signature*

5.2 Training SVM models

To measure the identification performance of the realised system, the testing and training data must be chosen from different data segments, which means that both training and testing data must be not the same. Therefore, after obtaining radar dataset, we randomised and divided them into two groups, 50% of them as a training set and the remaining 50% as a testing set. The model data is trained based on data that has been grouped already into each class (labelled data).

To have a better performance of the SVM classifier, before training and testing dataset, we need first an investigation to have a better SVM kernel by using cross-validation technique [20]. The fourth basic SVM kernel including the linear kernel, polynomial kernel, RBF kernel and Sigmoid kernel have been already investigated.

Basically, SVM kernel has two important parameters that are C and γ. Both parameters are used to control the over-fit weights and biases. Thus, before performing the process of training and testing data, it is important to have best parameters for C and γ, and then use them in training and testing processes, so that the classifier can

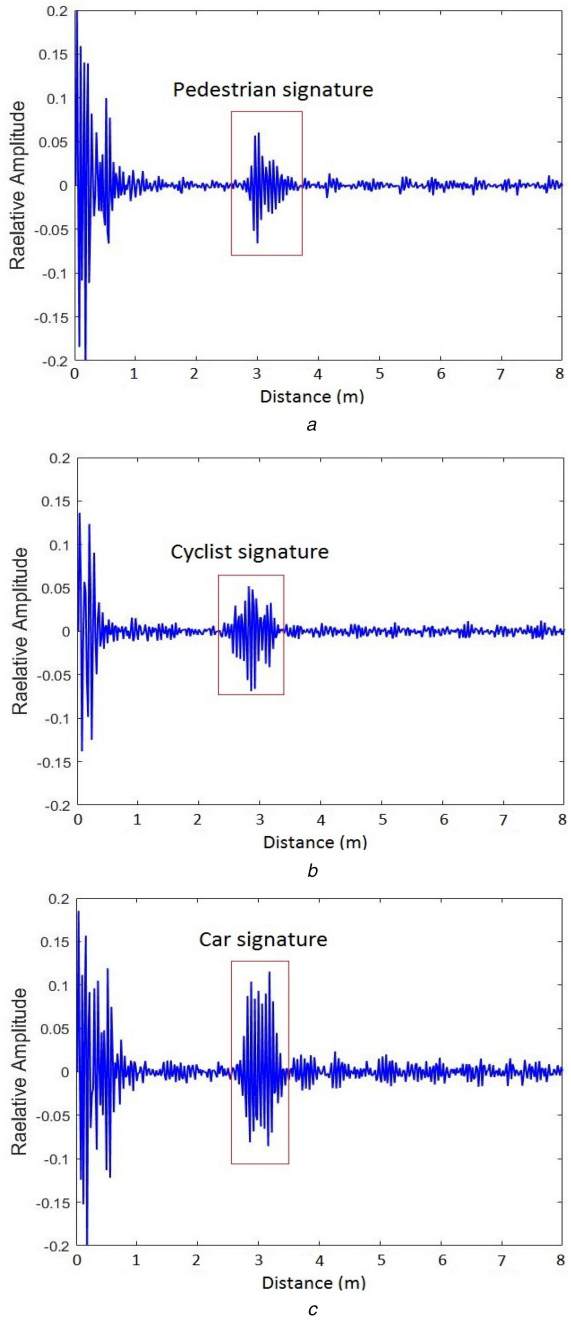

Fig. 13 *Signatures of the three different targets*
(a) Pedestrian signature, ***(b)*** Cyclist signature, ***(c)*** Car signature

predict more accurately the unknown data. A common strategy to have these parameters is to separate the training data into k equal size bins and then one bin is used as the validation for testing the model and the remaining of $k-1$ bins are used as the training data. The cross-validation process is then repeated k times (the folds), with each of the k bins used exactly once as the validation data. This technique is called k-fold cross-validation. The k results from the folds can then be averaged to produce a single estimation. The advantage of this method is that all observations are used for both training and validation, and each observation is used for validation exactly once. The best performance of accuracy (99.49%) is achieved at $C=4$ and $\gamma=2$. Table 4 shows the summary of best parameters for four used SVM kernels. Finally, we compared the performance of the four kernels by computing their cross-validation accuracy rates and we have chosen RBF kernel which has better performance for our model.

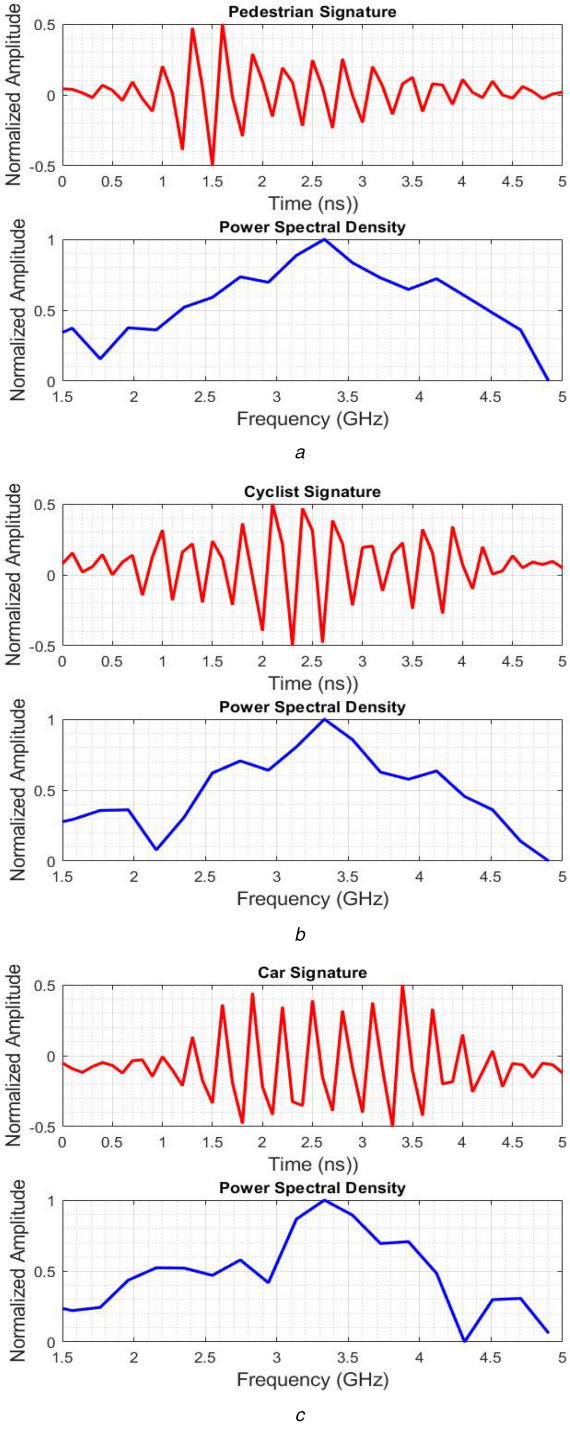

Fig. 14 *Normalised signatures of the three different targets followed by their power spectral densities. As can be seen, the figure shows that the different natures of the radar target yielded different radar signatures*
(a) Pedestrian signature and its power spectral density, ***(b)*** Cyclist signature and its power spectral density, ***(c)*** Car signature and its power spectral density

5.3 Testing SVM model

Before performing a real-time test, we have done first off-line testing; it means that we performed the evaluation by using the remaining of 50% dataset. Testing performance of the testing dataset will be predicted as a specific label based on the parameters obtained from the result of SVM training. Table 5 shows the performance of the confusion matrix of off-line testing SVM model.

The results show that the SVM gives a good performance for our system where the recognition rate is up to 96.23, 95.25 and 97.23% for the cyclist, pedestrian and car, respectively. It proves that the use of SVM in classification radar target for uncovered

Table 4 Best parameters for C and γ

SVM kernels	C	Gamma	Cross-validation accuracy, %
linear	128	—	95.64
polynomial	3.051758×10^{-5}	64	98.72
RBF	4	2	99.49
sigmoid	1024	0.0625	96.41

Table 5 Confusion matrix of using RBF kernel for three identification targets

	Cyclist, %	Pedestrian, %	Car, %
cyclist	96.23	2.46	1.31
pedestrian	3.62	95.25	1.13
car	1.60	1.17	97.23

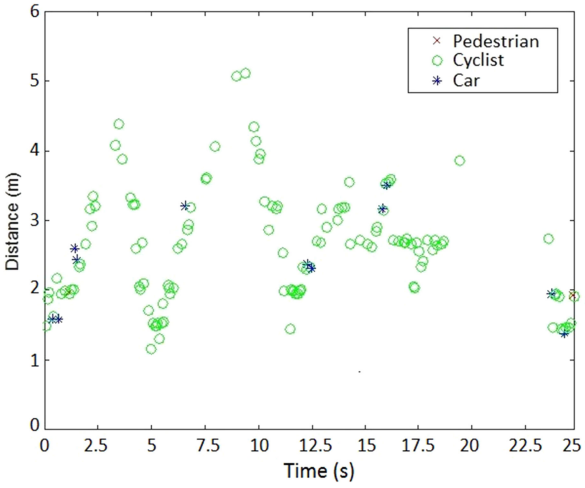

Fig. 15 *Real-time experiment result for investigating cyclist identification performance*

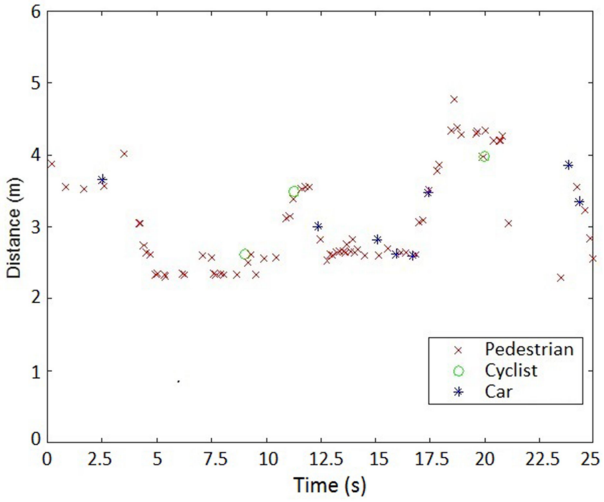

Fig. 16 *Real-time experiment result for investigating pedestrian identification performance*

road users such as cyclist and pedestrian results is very good in accuracy.

5.4 Real-time identification

Finally, we tested the ability of our UWB radar identification system to recognise the targets in real-time conditions. In this first experimentation, we performed the observation for every radar target independently, means that we have investigated their performances one by one.

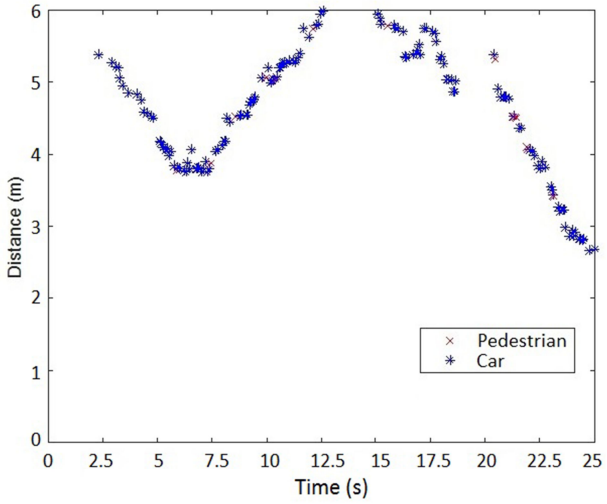

Fig. 17 *Real-time experiment result for investigating car identification performance*

Table 6 Confusion matrix of real-time identification radar target for three different natures: *cyclist*, *pedestrian* and *car*

	Cyclist, %	Pedestrian, %	Car, %
cyclist	92.77	6.38	0.85
pedestrian	6.76	90.82	2.42
car	0.0	9.27	90.73

We first investigated real-time identification for a cyclist. The performance of the result is shown in Fig. 15, where the system has successfully identified a cyclist as a cyclist with the accuracy of 92.77%. The second experiment was conducted for identifying a pedestrian, where the result performance is provided in Fig. 16. The system has successfully identified a pedestrian as a pedestrian with the accuracy of 90.82%. The final test was conducted for identifying a car. The system has successfully identified a car as a car with an accuracy of 90.73% as its performance is shown in Fig. 17. The confusion matrix for these experiments is summarised in Table 6.

6 Discussion and conclusion

This work is divided into two parts: the detection and recognition parts. The objective of the first part is to evaluate the performance of radar detectors in order to obtain a robust UWB radar detector, and the objective of the second part is to investigate the performance of the recognition system of SVM using the radar signature as input features.

In the first part of this work, we proposed to combine the HOS and the well known automatic CA-CFAR detector. There are two types of HOS algorithms, the fourth-order cumulant (Tugnait4 based) and the fourth-order cross-moment. First, we investigated both these algorithms to obtain the optimal performance of the HOS before combining with the CA-CFAR. On the basis of the investigation results, we found that both algorithms give a very similar performance in terms of noise suppression, but in terms of the complexity, the fourth-order cross-moment has less calculation than the fourth-order cumulant. This means that the fourth-order cross-moment is more efficient to be used in UWB radar. Then, we compared the performance of time-delay estimation between the fourth-order cross-moment and the ordinary second-order statistics. We noted that the performance of time-delay estimation of the fourth-order cross-moment is much better than that of the second-order statistics. Therefore, the fourth-order cross-moment has been considered to be used in our proposed UWB radar detector. Finally, by combining the fourth-order HOS and the CA-CFAR, an automatic UWB radar detector that is robust to the noise has been developed. To prove this idea, we have evaluated the performance between HOS with the fixed threshold value, CA-CFAR detector without time-delay estimation, and a combination of HOS and CA-

CFAR detector (the proposed method). The result is the combination of HOS and CA-CFAR promises a good performance for UWB radar detector.

In the second part of this work, we have investigated the performance of the recognition of SVM using the radar signature as input features. After investigating the performance of the proposed detector, we applied it to detect the positions of the radar targets. Once the position of the target is obtained, then we step back to the originally received echo and perform the windowing around the known target position and take it as a radar signature. As discussed in the recognition part, it has two important processes: training and testing. In the training process, it requires the features along with the labels associated with the class, where the features are taken to be trained. In this case, we have extracted 1000 signatures for each class including pedestrian, cyclist and car and 50% of them have been used as the training data and the rest of 50% have been used as data validation. The results show that the SVM gives a good performance for the proposed system, where the recognition rate is, respectively, up to 96.23, 95.25 and 97.23% for the cyclist, pedestrian and car. In the real testing performance using our scenarios, the system has successfully identified 92.77% of the right cyclist, 90.82% of the right pedestrian and 90.73% of the right car.

Preliminary results were encouraging and very useful for our future work. To enhance the performance of recognition, we will use deep belief network and also we will investigate the possibility to use a convolution neural network for UWB radar targets' recognition.

7 Acknowledgments

The present research work has been supported by the French National Agency for Research (ANR) through the project CYCLOPE. The authors gratefully acknowledge the support of this institution. We also thank the European Union, the French Government and the region Haut de France who have supported this work through ELSAT 2020 project (Ecomobility, Logistics, Security and Adaptability in Transport to 2020).

8 References

[1] Niewoehner, W., Alexander Berg, F.: 'Endangerment of pedestrians and bicyclists at intersections by right turning trucks' Proceedings – 19th International Technical Conference on the Enhanced Safety of Vehicles (ESV), Washington, DC, USA, June 2005, pp. 5–344

[2] Farooq, J.: 'Object detection and identification using SURF and BoW model'. Int. Conf. Computing, Electronic and Electrical Engineering (ICE Cube), Buttems, Quetta, Pakistan, April 2016, pp. 318–323

[3] Hamidoun, K., Elassali, R., Elhillali, Y., *et al.*: 'A new multi-user ultra wide band system based on modified Gegenbauer functions and M-OAM modulation for communication of intelligent transportation systems', *Wirel. Pers. Commun.*, 2015, **82**, (4), pp. 2115–2134

[4] Sakkila, L., Elhillali, Y., Zaidouni, J., *et al.*: 'High order statistic receiver applied to UWB radar'. IEEE Pacific Rim Conf. Communications, Computers and Signal Processing PacRim 2009, Victoria, BC, August 2009, pp. 643–647

[5] Damien, S.: '*OFCOM infomailing no. 8*' (Federal Office of Communication, Switzerland, 2007), pp. 11–15

[6] Sakkila, L., Rivenq, A., Boukour, F., *et al.*: 'Collision avoidance radar system using UWB waveforms signature for road applications'. 2009 Ninth Int. Conf. Intelligent Transport Systems Telecommunications (ITST), Lille, France, 2009, pp. 223–226

[7] Qasim, S.M., Khan, A.A., Alshebeili, S., *et al.*: 'FPGA based architecture for the computation of fourth-order cross moments'. 2007 Int. Conf. Intelligent and Advanced Systems, Kuala Lumpur, 2007, pp. 1400–1403

[8] Mendel, J.M.: 'Tutorial on higher-order statistics (spectra) in signal processing and system theory: theoretical results and some applications', *Proc. IEEE*, 1991, **79**, (3), pp. 278–305

[9] Sanullah, M.: 'A review of higher order statistics and spectra in communication systems', *Global J. Sci. Front. Res. Phys. Space Sci.*, 2013, **13**, (4), available at: https://journalofscience.org/index.php/GJSFR/article/view/807 Accessed July 2017

[10] Tugnait, J.K.: 'Time delay estimation with unknown spatialy correlated Gaussian noise', *IEEE Trans. Signal Process.*, 1993, **42**, (2), pp. 549–558

[11] Byun, H., Seong-Whan Lee, S-W.: 'Applications of support vector machines for pattern recognition: a survey'. SVM 2002, Berlin, Germany, 2002 (**LNCS 2388**), pp. 213–236

[12] Hsu, C.-W., Chang, C.-C., Lin, C.-J.: '*A practical guide to support vector classification*' (Department of Computer Science National Taiwan University, Taipei 106, Taiwan)

[13] Chang, C.-C., Lin, C.-J.: 'LIBSVM: a library for support vector machines'. *ACM Transactions on Intelligent Systems and Technology*, 2011, **2**, (3), pp. 2:27:1–27:27. Software available at http://www.csie.ntu.edu.tw/cjlin/libsvm, accessed February 2017

[14] UMAIN.Inc: 'User's manual HST-D3 evaluation kit with Raspberry Pi 3 development version. Doc no. HST-D3_Manual_V1.9.3_ENG', 2017. Manual available at http://www.umain.co.kr, accessed December 2017

[15] Ewell, G.W.: 'Design of digital moving target indication radar processors'. PhD thesis, Georgia Institute of Technology, April 1974

[16] Meikle, H.: '*Modern radar systems*' (Artech House, 2008)

[17] Galushko, V.G.: 'Analysis of the CA-CFAR algorithm as applied to detection of stationary Gaussian signals against a normal noise background'. 2016 Ninth Int. Kharkiv Symp. Physics and Engineering of Microwaves, Millimeter and Submillimeter Waves (MSMW), Kharkiv, 2016, pp. 1–3

[18] Richards, M.A.: '*Fundamentals of radar signal processing*' (McGraw-Hill, New York, 2005)

[19] 'Constant false-alarm rate (CFAR) detectors'. Available at https://fr.mathworks.com/help/phased/examples/constant-false-alarm-rate-cfar-detection.html, accessed June 2018

[20] Liu, J., Fang, N., Xie, Y.J., *et al.*: 'Radar target classification using support vector machine and subspace methods', *IET Radar Sonar Navig.*, 2015, **9**, (6), pp. 632–640